Nuclear Instruments and Methods in Physics Research A 613 (2010) 218–225

Contents lists available at ScienceDirect

Nuclear Instruments and Methods in Physics Research A

journal homepage: www.elsevier.com/locate/nima

Lifetime effects for high-resolution gamma-ray spectroscopy at relativistic energies and their implications for the RISING spectrometer

P. Doornenbal [a,b,*], P. Reiter [a], H. Grawe [b], T. Saito [b], A. Al-Khatib [c], A. Banu [b], T. Beck [b], F. Becker [b], P. Bednarczyk [b,d], G. Benzoni [e], A. Bracco [e,f], A. Bürger [c], L. Caceres [b,g], F. Camera [e,f], S. Chmel [c,1], F.C.L. Crespi [e,f], H. Geissel [b], J. Gerl [b], M. Górska [b], J. Grębosz [b,d], H. Hübel [c], M. Kavatsyuk [b,h], O. Kavatsyuk [b,h], M. Kmiecik [d], I. Kojouharov [b], N. Kurz [b], R. Lozeva [b,i,2], A. Maj [d], S. Mandal [j], W. Meczynski [d], B. Million [e], Zs. Podolyák [k], A. Richard [a], N. Saito [b], H. Schaffner [b], M. Seidlitz [a], T. Striepling [a], J. Walker [b], N. Warr [a], H. Weick [b], O. Wieland [e], M. Winkler [b], H.J. Wollersheim [b]

[a] Institut für Kernphysik, Universität zu Köln, 50937 Köln, Germany
[b] GSI Helmholtzzentrum für Schwerionenforschung GmbH, 64291 Darmstadt, Germany
[c] Helmholtz-Institut für Strahlen- und Kernphysik, Universität Bonn, 53115 Bonn, Germany
[d] The Niewodniczanski Institute of Nuclear Physics, Polish Academy of Sciences, 31-342 Krakow, Poland
[e] INFN Sezione di Milano, 20133 Milano, Italy
[f] Dipartimento di Fisica, Università di Milano, 20133 Milano, Italy
[g] Departamento de Física Teórica, Universidad Autonoma de Madrid, 28049 Madrid, Spain
[h] Taras Shevchenko Kiev National University, 03680 Kiev, Ukraine
[i] Faculty of Physics, St. Kliment Ohridski University of Sofia, 1164 Sofia, Bulgaria
[j] Department of Physics and Astrophysics, University of Delhi, Delhi 110 007, India
[k] Department of Physics, University of Surrey, Guildford GU2 7XH, UK

ARTICLE INFO

Article history:
Received 30 October 2009
Accepted 4 November 2009
Available online 11 November 2009

Keywords:
In-beam γ−ray spectroscopy
Lifetime measurement techniques

ABSTRACT

The lineshapes and peak position of Doppler corrected γ−ray spectra from in-beam experiments at relativistic energies are investigated with respect to the intrinsic energy resolution of the employed detectors, the particles' velocities, and the photons' emission angle uncertainties at the moment of γ−ray emission. The uncertainties in velocity and photon emission angle are dependent on the lifetime of the excited state. The impact of these two observables on the lineshape and energy resolution are studied for the RISING γ−spectrometer by means of simulations and experimental results from a two-step fragmentation experiment at $\approx 200\,\mathrm{MeV}/u$. Potential use of the distinct lineshape for lifetime determination is demonstrated for measured γ−ray transitions.

1. Introduction

In recent years, the development of in-beam γ−ray spectroscopy of radioactive ion beams from in-flight facilities at relativistic energies has enabled nuclear structure investigations that were previously beyond reach. In these experiments, rare isotope facilities provide in-flight separated beams with relativistic velocities in the range of $0.3 \leq \beta \leq 0.8$ after primary fragmentation reactions, which are incident on a secondary target to induce reactions such as Coulomb excitation or knockout reactions [1,2]. A decisive advantage of this method is given by the beam's high energy. Thick secondary reaction targets can be employed due to the low energy loss at these beam energies, compensating very low secondary beam rates.

The emitted γ−rays from decaying excited states are substantially Doppler shifted in the laboratory frame, which requires a back transformation of the γ−ray energy into the nuclei's rest frame system. The achievable energy resolution after the Doppler correction depends mainly on the following factors: (i) the intrinsic detector energy resolution, (ii) the effective opening angle of the utilized γ−ray detectors, (iii) the accuracy of the position and velocity determination of the heavy ion at the moment when the γ−ray decay occurs. Position measurements of the individual beam particles are mandatory to track the heavy ions' paths in front of and behind the reaction target. Due to forward peaked small scattering angles at relativistic energies an accurate transversal position determination of the γ−ray decay

* Corresponding author. Present address: RIKEN Nishina Center for Accelerator-Based Science, 2-1 Hirosawa, Wako, Saitama 351-0198, Japan.
E-mail address: pieter@ribf.riken.jp (P. Doornenbal).
[1] Present address: Fraunhofer INT, Euskirchen, Germany.
[2] Present address: CSNSM, Universitè Paris-Sud 11, CNRS/IN2P3, F-91405 Orsay–Campus, France.

0168-9002/$ - see front matter © 2009 Elsevier B.V. All rights reserved.
doi:10.1016/j.nima.2009.11.017

point in the plane perpendicular to the beam axis is obtained. However, the longitudinal position determination along the beam axis depends on the reaction target's thickness and the lifetime of the excited state. Moreover, the velocity of the heavy ions at the γ−ray emission time is needed. Velocity measurements are also necessary before and after passing the secondary target as the secondary beam has generally a considerable momentum spread. The accuracy of the velocity determination is heavily affected by the lifetime of the excited state and the thickness of the reaction target. A considerable fraction of γ−ray decays can occur during the slowing down process within the target. As a consequence, the exact velocity at the moment of γ−ray emission stays uncertain, causing an imperfect Doppler correction, i.e., a broadening and a specific lineshape of the Doppler corrected γ−ray peaks.

To which extent the lineshape of a γ−ray peak is affected depends not only on the excited state's lifetime but is closely related to the geometry of the specific γ−ray detection array and experimental setup. In this paper, we will focus on lifetime effects for in-beam γ−ray spectroscopy with the RISING array [3], operated at the S4 focal plane of the fragment separator FRS [4] at GSI, Darmstadt. This experimental setup employs high resolution in-beam spectroscopy at the highest velocities to date. We commence with general remarks on the Doppler shift correction for in-beam γ−ray spectroscopy. Monte-Carlo simulations are performed to study and disentangle the different contributions to the line shape of the γ−ray peaks. Finally, experimental lineshapes from in-flight decay at $\approx 200\,\mathrm{MeV}/u$ kinetic energy after secondary fragmentation reactions are compared to simulations.

2. General remarks on the Doppler correction

Gamma-rays emitted from excited nuclei moving at relativistic energies are strongly Doppler shifted. The detected γ−ray energy E_γ in the laboratory frame is related to the transition energy $E_{\gamma 0}$ in the rest frame by the Doppler formula through:

$$\frac{E_\gamma}{E_{\gamma 0}} = \frac{\sqrt{1-\beta^2}}{1-\beta\cos\vartheta_\gamma}. \tag{1}$$

Here, ϑ_γ is the angle between the emitting particle and the emitted γ−ray in the laboratory frame, respectively. The resulting energy resolution after performing the Doppler correction of measured γ−ray energies E_γ is given by

$$\left(\frac{\Delta E_{\gamma 0}}{E_{\gamma 0}}\right)^2 = \left(\frac{\beta\sin\vartheta_\gamma}{1-\beta\cos\vartheta_\gamma}\right)^2 (\Delta\vartheta_\gamma)^2 + \left(\frac{\beta-\cos\vartheta_\gamma}{(1-\beta^2)(1-\beta\cos\vartheta_\gamma)}\right)^2 (\Delta\beta)^2 + \left(\frac{\Delta E_{\mathrm{intr}}}{E_\gamma}\right)^2. \tag{2}$$

Three factors determine the energy resolution after applying the Doppler shift correction: (i) angular uncertainty between particle and photon $\Delta\vartheta_\gamma$, (ii) beam velocity uncertainty $\Delta\beta$, and (iii) intrinsic energy resolution of the γ−ray detector ΔE_{intr}. The first two uncertainties in the γ−ray emission angle ϑ_γ and the beam velocity are affected by the lifetime of the decaying states.

2.1. Angular uncertainty between particle and photon $\Delta\vartheta_\gamma$

Data on three points is required to reconstruct the angle ϑ_γ. These are (i) the position of the particle at the moment of γ−ray emission, (ii) the position of the emitting particle downstream of the target, and (iii) the position of the detected γ−ray. With this information two vectors are created spanning the angle ϑ_γ.

For thin targets and short lifetimes, the finite size of the γ- ray detectors yields the major contribution to the uncertainty $\Delta\vartheta_\gamma$. To obtain the point of γ−ray decay, a suited method is to utilize a position sensitive target. Elsewise position sensitive detectors are used for tracking the individual beam particles upstream or downstream the target to reconstruct the reaction position. As the scattering angles of the particles are typically small ($\leq 4^\circ$) at relativistic energies, the position information perpendicular to the beam axis can be obtained with good accuracy. For the z-coordinate along the beam axis only the target position itself can be used as an assumption for the z-coordinate of the γ−ray decay and the reaction points. Typical target thicknesses are in range of a few hundred $\mathrm{mg/cm^2}$ up to several $\mathrm{g/cm^2}$. If low density targets such as liquid hydrogen ($\rho = 70\,\mathrm{mg/cm^3}$) are used in the experiment, the target thickness along the beam axis may even reach several cm.

As the z-coordinate of the reaction point inside the target cannot be determined, thick targets contribute to a considerable amount to the uncertainty $\Delta\vartheta_\gamma$, in particular for detectors placed at 90°. Moreover, the uncertainty in $\Delta\vartheta_\gamma$ for the Doppler shift correction is increased by the lifetime of the excited state. The particles move along the beam axis away from the target position before emitting γ−rays, thereby changing ϑ_γ. Taking into account the time t in the moving system between excitation and decay of a nuclear state and neglecting the velocity change due to energy loss inside the target, the position of the γ−ray decay along the beam axis in the laboratory system shifts by $z_\gamma = t\beta\gamma c$, which will consequently alter the angle ϑ_γ. This change in angle cannot be corrected on an event-by-event basis. For a known lifetime the mean z-coordinate of the decay position $\langle z_\gamma \rangle = T_{1/2}\beta\gamma c/\ln 2$ has to be taken into account for the Doppler correction (the target center is $z=0$). The mean decay position for three different beam velocities are shown as a function of the halflife in Fig. 1. For long halflives of more than 50 ps, which are common for $E(2_1^+)$ levels in regions of deformations in the nuclear chart, $\langle z_\gamma \rangle$ shifts by several cm. Typically, γ−ray spectrometers have distances of several tens of cm to the target. Therefore, such a shift in decay position is considerable and illustrated in Fig. 2 for three halflives of 100, 200, and 300 ps at a beam velocity of $100\,\mathrm{MeV}/u$. The decay position distribution along the z-axis cannot be accounted for in the Doppler correction and affects the obtainable energy resolution of the experiment.

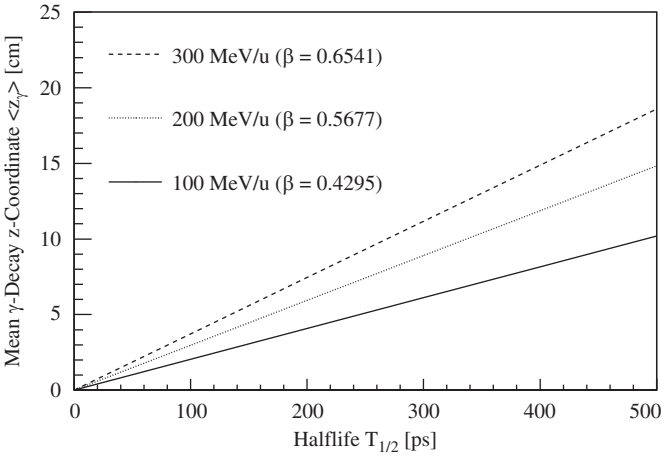

Fig. 1. Mean z-coordinate of the decay position $\langle z_\gamma \rangle$ as a function the excited state's halflife for three different secondary beam velocities. See text for details.

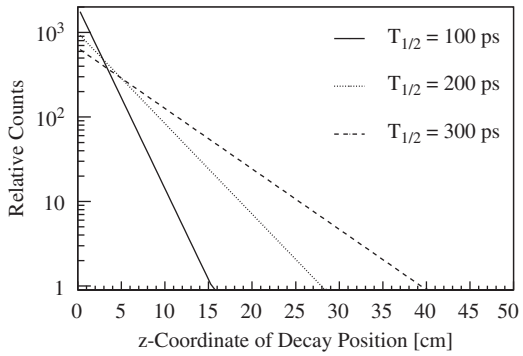

Fig. 2. z-coordinate distribution of the heavy ions' position with an energy of 100 MeV/u at the moment of γ−ray emission and halflives of an excited state of 100 (solid line), 200 (dotted line), and 300 ps (dashed line), respectively.

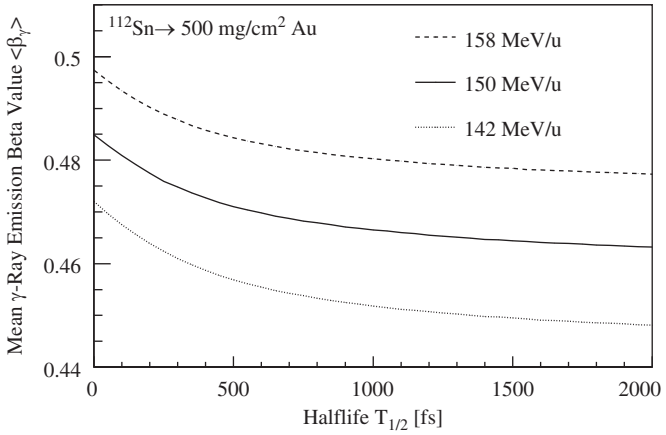

Fig. 3. Mean velocity at the moment of γ−ray emission $\langle\beta_\gamma\rangle$ as a function of the halflife of an excited state for a ^{112}Sn beam impinging on a 500 mg/cm^2 ^{197}Au target at energies of 142 (dotted line), 150 (solid line), and 158 MeV/u (dashed line), respectively. See text for details.

2.2. Beam velocity uncertainty $\Delta\beta$

While penetrating the target, the beam and its fragmentation products undergo an energy loss, which is well described by theoretical work [5]. Depending on the ratio between the lifetime of an excited state and the transmission time necessary to penetrate the target, i.e., its thickness, the γ−ray decay will occur either predominantly inside or behind the target. In the latter case, the velocity at the moment of γ−ray decay can be deduced from a velocity (time-of-flight) measurement after the target. In many cases, however, a considerable amount of decays will occur inside the target. Consequently, the exact velocity at the moment of γ−ray emission cannot be determined. In these cases, the Doppler correction must be done with an average velocity $\langle\beta_\gamma\rangle$ of the particle at the moment of γ−ray emission assuming a certain lifetime of the excited state (unless it is known). However, for a given halflife, $\langle\beta_\gamma\rangle$ depends on the incoming beam velocity. To perform an event-by-event based Doppler correction, every measured velocity before reaching (bt) or after leaving (at) the target, $\beta_{\mathrm{bt/at}}$, must be correlated with its according $\langle\beta_\gamma\rangle$ from simulation.

Because the stopping power dE/dX depends on several parameters, the impact of the velocity uncertainty for the event-by-event Doppler correction is illustrated by a typical example. For a beam of ^{112}Sn impinging on a 500 mg/cm^2 ^{197}Au target at energies of 142, 150, and 158 MeV/u Fig. 3 displays $\langle\beta_\gamma\rangle$ as a function of the halflife of an excited state. A constant excitation cross-section along the nuclei's path through the target and no momentum spread of the beam for the different energies is assumed in the simulations. The $\langle\beta_\gamma\rangle$ separation for the different lines becomes slightly larger with increasing halflife. For short halflives the change in $\langle\beta_\gamma\rangle$ is most pronounced. Excited states with halflives of $\geq$1000 fs decay predominantly after the target. For these cases, $\langle\beta_\gamma\rangle$ almost matches the velocity after the target. A different pattern is observed for low atomic number Z, low density targets, as ^{9}Be. Due to the higher stopping power of Be in units of MeV/mg/cm^2, the energy loss in a 500 mg/cm^2 ^{197}Au target for a ^{112}Sn beam at 150 MeV/u is equal to the energy loss in a 315 mg/cm^2 ^{9}Be target. Be has a much lower density ($\rho = 1.85$ g/cm^3 compared to $\rho = 19.3$ g/cm^3 for Au) and $\langle\beta_\gamma\rangle$ changes considerably up to longer halflives of several ps, as shown in Fig. 4.

For secondary beams with momentum distribution the mean velocity at the moment of γ−ray emission $\langle\langle\beta_\gamma\rangle\rangle$ corresponds to the mean velocity before or after the target, $\langle\beta_{\mathrm{bt/at}}\rangle$. The difference between $\beta_{\mathrm{bt/at}}$ to the respective mean value of the distribution, $\langle\beta_{\mathrm{bt/at}}\rangle$, can be correlated with the difference of the corresponding $\langle\beta_\gamma\rangle$ and the mean velocity at the moment of γ−ray emission, i.e., $\langle\langle\beta_\gamma\rangle\rangle$, of the distribution. In Fig. 5 this is shown for halflives of 0, 500, and 1000 fs and the ^{112}Sn beam

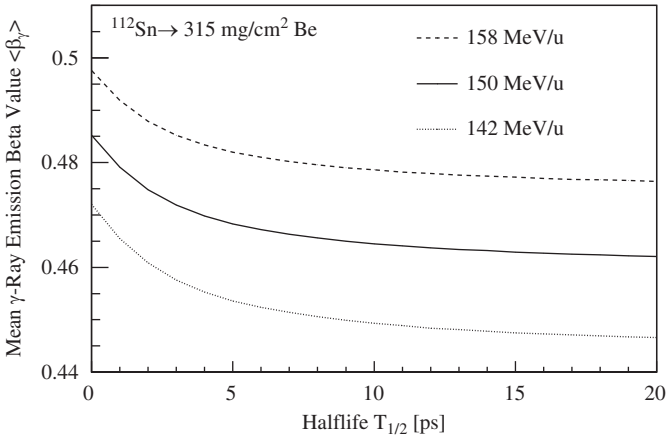

Fig. 4. Mean velocity at the moment of γ−ray emission $\langle\beta_\gamma\rangle$ as a function of the halflife of an excited state for a ^{112}Sn beam impinging on a 315 mg/cm^2 ^{9}Be target at energies of 142, 150, and 158 MeV/u, respectively. See text for details.

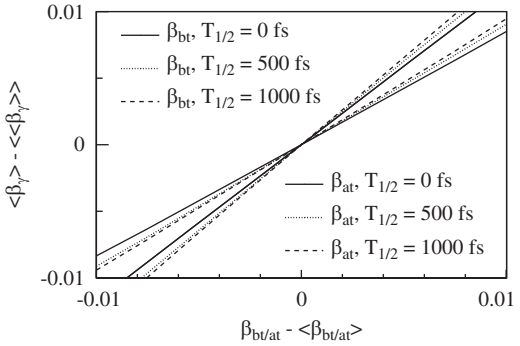

Fig. 5. Relation between the difference of the velocity before/after the secondary target β_{bt}/at and its mean value $\langle\beta_{\mathrm{bt}}/\mathrm{at}\rangle$ and the respective mean velocities at the moment of γ−ray decay, $\langle\beta_\gamma\rangle$ and $\langle\langle\beta_\gamma\rangle\rangle$. The calculations were performed for a ^{112}Sn beam with an average velocity of 150 MeV/u impinging on a 500 mg/cm^2 ^{9}Be target and halflives of 0, 500, and 1000 fs, respectively.

hitting the ^{197}Au target. The result are straight lines, their slope α increasing slightly with increasing halflife. For thin targets, i.e., only very little energy change, α is close to unity. If the velocity is measured before the target, α must be greater than one, for measurements after the target, it must be smaller than one. The slope α can be used for an event-by-event Doppler correction using the equation:

$$\beta_{Doppler} = \langle\langle\beta_\gamma\rangle\rangle + \alpha \times (\beta_{bt/at} - \langle\beta_{bt/at}\rangle). \quad (3)$$

The combined consequences of the z-coordinate and velocity uncertainty on the γ−ray energy resolution and efficiency in a real experiment will be demonstrated and discussed in the following sections. The obtained results are based on Monte-Carlo simulations and on experimental investigations performed with the RISING setup [3] at GSI, Darmstadt.

3. The RISING setup

RISING combines the fragment separator FRS [4] at GSI with a γ−ray spectrometer to observe decays from excited states of exotic nuclei. The Fast Beam setup of RISING consists of three sub-arrays: 15 Cluster High Purity Ge detectors [7], eight MINIBALL High Purity Ge detectors [8], and eight Hector BaF_2 detectors [9,10]. Details of the experimental setup and particle identification before and after passing the secondary target can be found for example in Refs. [3,4,6]. Here, it is sufficient to know that the energy spread of the heavy ions in front of the secondary target is measured by the time-of-flight between two scintillation detectors. The outgoing particle direction and the reaction point are determined via position sensitive Si detectors mounted directly after the secondary target and 1400 mm downstream.

The γ−ray detectors are mounted at different angles and distances, as shown schematically in Fig. 6. The Cluster detectors, each containing seven individually encapsulated crystals, are positioned at the most forward angles in three rings of 16°, 33°, and 36°. They can be placed at distances between 700 and 1400 mm to the secondary target. The six-fold segmented MINIBALL triple detectors are arranged in two rings of 51° and 85° and can be positioned at distances varying between 200 and 400 mm. The BaF_2 detectors are situated at angles of 85° and 142° and distances of 350 mm.

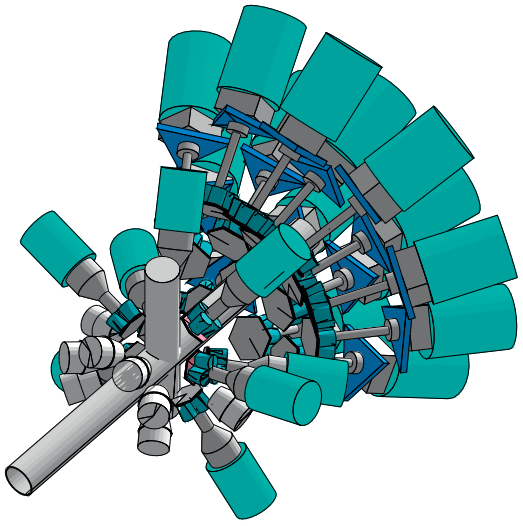

Fig. 6. (Color online) Schematic drawing of the RISING Fast Beam array. For references and details see text.

4. Lineshape simulations of the RISING setup

The lineshape and energy resolution after applying the Doppler correction are investigated via Monte-Carlo simulations for the two types of high-resolution RISING detectors, the MINIBALL and the Cluster detectors. The GEANT4 simulation package [11] is employed. As before, the lineshape caused by $\Delta\vartheta_\gamma$ and $\Delta\beta$ are discussed separately. The detectors are placed in close geometry, i.e., the distance of the Cluster detector front side to the target is 700 mm and the distance of the MINIBALL detector front side is 200 mm. The MINIBALL detectors are six fold segmented allowing a better localization and position determination for the incoming γ−ray. Only events with an interaction in solely one crystal for the Cluster detectors or solely one segment for the MINIBALL detectors are accounted for.

4.1. Lineshape due to de-excitation along the beam axis

Neglecting the energy loss in the target, the distance traveled by the particles between excitation and de-excitation depends on the velocity and on the lifetime of the excited state. In the simulations, a γ−ray of 500 keV is emitted at a beam energy of 100 MeV/u and halflives from 0 to 100 ps are assumed. Fig. 7 shows the resulting lineshapes, which are caused by the

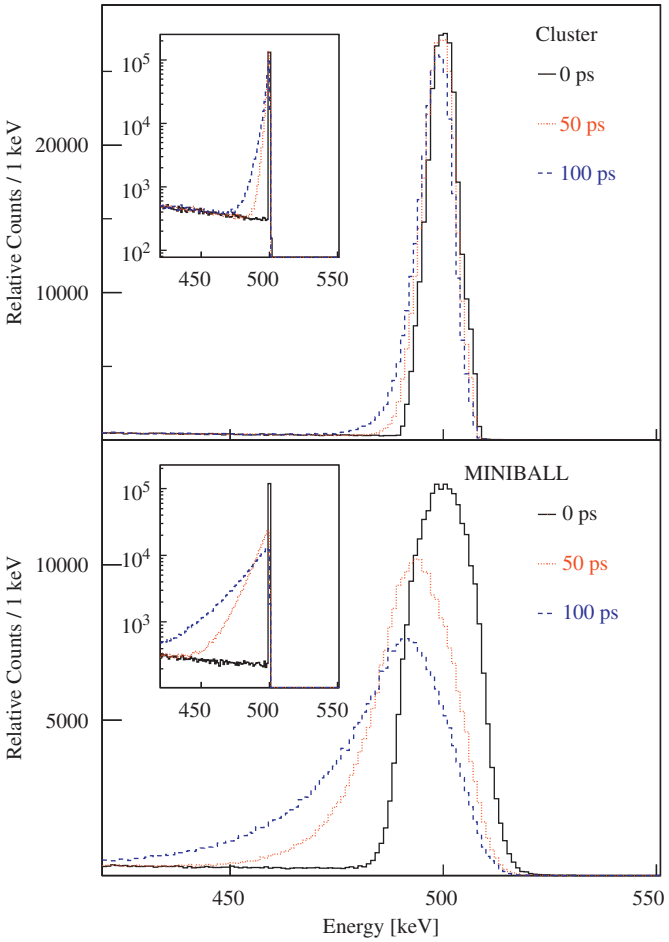

Fig. 7. Simulated Doppler corrected detector response for the Cluster (upper panel) and MINIBALL detectors (lower panel) for a γ−ray of 500 keV emitted at 100 MeV/u for three different halflife values of 0 (black solid), 50 (red dotted), and 100 ps (blue dashed). The insets show the detector response when the uncertainty of the detector's opening angles and the intrinsic resolution are disregarded in the simulation. (For interpretation of the references to the color in this figure legend, the reader is referred to the web version of this article.)

broadening due to the opening angle of the detector and the lifetime of the decaying state. For the Doppler correction, γ−ray emission at the middle of the target ($\langle z_\gamma \rangle = 0$) is assumed. For $T_{1/2} = 0$ ps the centroid of the peak distribution lies at 500 keV. As $T_{1/2}$ increases, the centroid of the distribution shifts to lower energies. This is caused by the increase in angle between the γ−ray detectors and the beam particle trajectory, leading to an exponential tail towards lower energies. The reason of this behavior can be demonstrated by neglecting the Doppler broadening due to the detectors' opening angles in the simulation, as depicted in the insets of Fig. 7. To achieve this, the simulated first interaction point of the γ−ray in the detectors' crystals is used for the Doppler correction.

The peak position shift depends on the position and distance of the γ−ray detectors. For a fixed distance to the target, the shift shows a maximum where the derivative of the square root of the first term in Eq. (2), given by

$$\frac{d}{d\vartheta_\gamma}\frac{\beta\sin\vartheta_\gamma}{1-\beta\cos\vartheta_\gamma} = \frac{\beta(\cos\vartheta_\gamma - \beta)}{(1-\beta\cos\vartheta_\gamma)^2} \tag{4}$$

is zero. This is the case for $\cos\vartheta_\gamma = \beta$, yielding values of 65°, 55°, and 49°, for energies of 100, 200, and 300 MeV/u. As the MINIBALL detectors are located in close distance to the target and all the individual segments cover ϑ−angles in the range from 41° to 101°, they are very sensitive to decays along the beam axis. On the other hand, the Cluster detectors are less affected due to the small ϑ−angles and large distances of the crystals to the target. This explains the considerable difference between the two detector groups in Fig. 7.

A linear dependence between the shift of the centroid of the peak position and the halflife of the excited state is obtained as a result. The relative energy shift, given in %, is shown in Fig. 8 as a function of the excited state's halflife for a beam energy of 100 MeV/u.

4.2. Lineshape due to γ- ray decay during the deceleration inside the target

The second major contribution to the lineshape of the γ−ray peaks is caused by the fact that γ−ray decay may occur during the emitting particles' deceleration in the target. Here the uncertainty

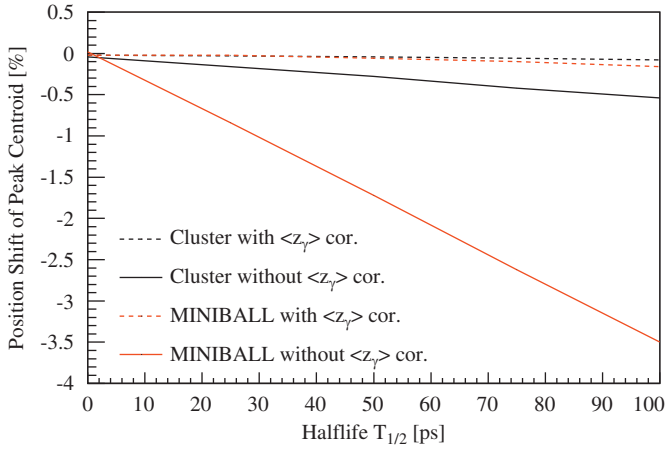

Fig. 8. Position shift of the peak centroid after applying the Doppler correction as a function of the halflife of the excited state at 100 MeV/u for the Cluster (thin black) and MINIBALL detectors (thick red). The shown Doppler corrections are applied with and without taking the centroid decay position into account. In the latter case (solid lines) $\langle z_\gamma \rangle = 0$ is assumed, while in the former the $\langle z_\gamma \rangle$ value as depicted in Fig. 1 is used. (For interpretation of the references to the color in this figure legend, the reader is referred to the web version of this article.)

$\Delta\beta$ depends on the specific combination of target, beam nuclei, beam energy, and halflife of the excited state. Lineshape effects are demonstrated quantitatively by the specific example of a ^{112}Sn beam impinging at 150 MeV/u on a 500 mg/cm^2 ^{197}Au target, like in Section 2.2. The simulated $2_1^+ \rightarrow 0_{g.s.}^+$ decay with an energy of 1256.85 keV [12] is reflecting the de-excitation process after a direct one step Coulomb excitation reaction. An accepted halflife of $T_{1/2} = 0.37(2)$ ps [12] can be used for the decay. To demonstrate lifetime effects, we vary the halflife and simulate the decay with halflives of $0.5 \cdot T_{1/2}$, $1 \cdot T_{1/2}$, and $2 \cdot T_{1/2}$, i.e., 185, 370, and 740 fs, respectively.

The velocity or β distributions at the moment of γ−ray emission are shown in Fig. 9. The number of γ−rays emitted after the target increases with increasing lifetime causing the unique value of $\beta_{at} = 0.46$ at low velocities for all three cases. In case Doppler correction is applied using the measurable β_{at}−value, energies from γ−rays decaying after the target will be shifted to the proper energy. Decays within the target are shifted to wrong energies according to the spread in velocity reflected in the second term of Eq. (2).

Generally, if $\cos\vartheta_\gamma > \beta_\gamma$, the resulting energy shift will be towards too high energies, while for $\cos\vartheta_\gamma < \beta_\gamma$ the shift will be towards too low energies. The Doppler corrected spectra of the ^{112}Sn transition for the Cluster and MINIBALL detectors are shown in Fig. 10. As the Cluster detectors occupy low ϑ_γ angles, a tail towards high energies occurs. The MINIBALL detectors are positioned around $\cos\vartheta_\gamma = \beta_\gamma$ and only a minor influence from $\Delta\beta_\gamma$ is visible. The insets of Fig. 10 illustrate again the lineshape for the case when the opening angle Doppler broadening and intrinsic energy resolution are disregarded in the simulation. As expected, the lineshape of the Cluster detectors resembles the β_γ distribution and Doppler corrected γ−ray energies are shifted up to 10% above the transition energy. For the MINIBALL detectors the effect is much smaller and almost symmetric, as shifts towards lower and higher energies are involved. The ratio of observed correct peak to tail ratio corresponds exactly to the ratio of γ−ray decays occurring after or within the target. Therefore, a precise determination of the lineshape, especially the asymmetry of the peak, enables a measure of the lifetime of an excited state.

The peak centroid deviation from the correct transition energy after applying the Doppler correction using β_{at} is shown in Fig. 11 as a function of the halflife of the excited state. For this particular projectile, beam energy, and target combination, only the Cluster detectors are affected. With measurable β_{at}−values after the target the Doppler corrected transition energy deviates from the correct value up to more than 2%. A Doppler correction using $\langle \beta_\gamma \rangle$ for 150 MeV/u from Fig. 3 shifts the energy centroid towards the proper

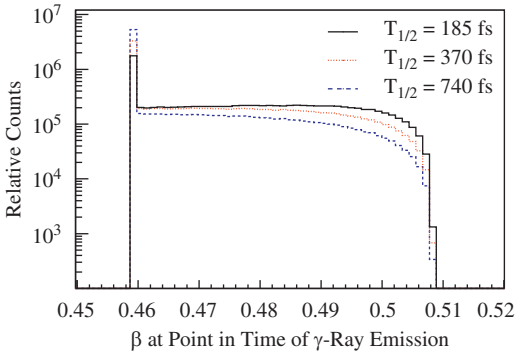

Fig. 9. β- distribution at the moment of γ−ray emission for a ^{112}Sn beam impinging at 150 MeV/u on a 500 mg/cm^2 ^{197}Au target and halflives of 185 (black solid), 370 (red dotted), and 740 fs (blue dashed), respectively. (For interpretation of the references to the color in this figure legend, the reader is referred to the web version of this article.)

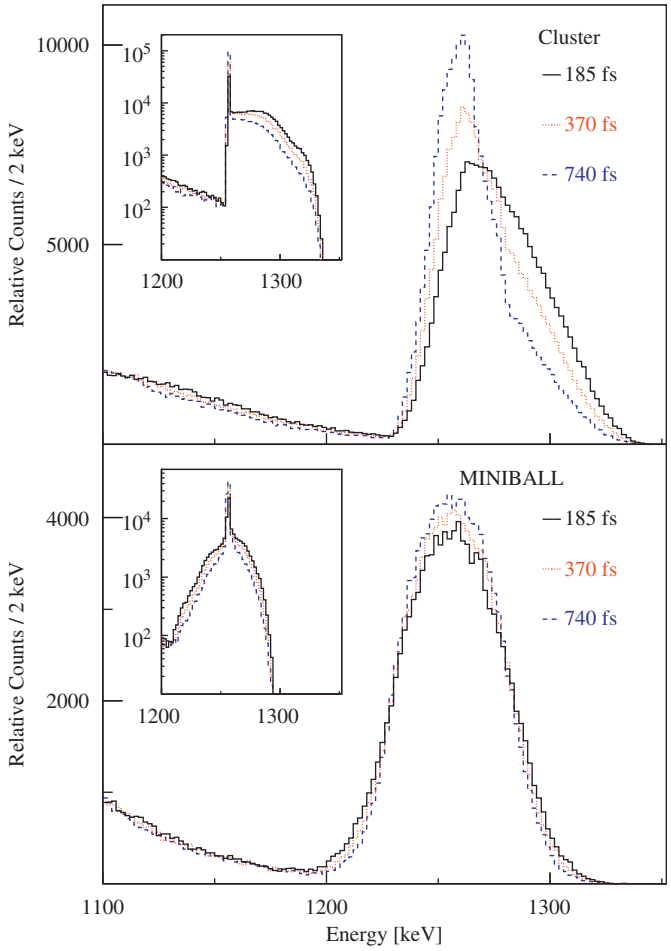

Fig. 10. Simulated Doppler corrected detector response for the Cluster (upper panel) and MINIBALL detectors (lower panel) for the $2_1^+ \rightarrow 0_{g.s.}^+$ of ^{112}Sn. The ^{112}Sn beam is impinging at 150 MeV/u on a 500 mg/cm^2 ^{197}Au target and halflives of 185 (black solid), 370 (red dotted), and 740 fs (blue dashed), respectively, are assumed. The insets show the detector response when the uncertainty of the detector's opening angles and their intrinsic resolution are "turned off". The Doppler correction is performed using β_{at}. (For interpretation of the references to the color in this figure legend, the reader is referred to the web version of this article.)

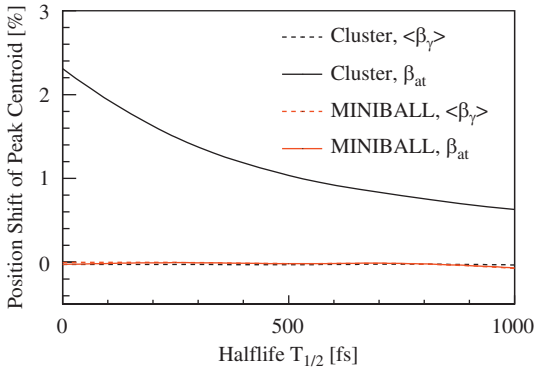

Fig. 11. Deviation of observed peak position after applying a Doppler correction using $\langle\beta_\gamma\rangle$ (dashed lines) and β_{at} (solid lines) for the Cluster (black thin) and MINIBALL (red thick) detectors. The ^{112}Sn projectile impinged at 150 MeV/u on a 500 mg/cm^2 ^{197}Au target. (For interpretation of the references to the color in this figure legend, the reader is referred to the web version of this article.)

position. Therefore, without presumption of the lifetime of the de-excitation γ−ray, the transition energy assignment is limited to a precision of $\pm 1\%$ from the Cluster detectors alone in this case.

5. Experimental results

Lineshapes of the $1_1^+ \rightarrow 0_{g.s.}^+$ decay in ^{34}Cl and the $3/2_1^+ \rightarrow 1/2_{g.s.}^+$ decay in ^{31}S were investigated experimentally, exploiting the two-step fragmentation technique. A primary beam of ^{40}Ca at an energy of 420 MeV/u was provided by the heavy ion synchrotron SIS and impinged on a ^{9}Be target with 4 g/cm^2 thickness. From the primary reaction products ^{37}Ca was selected and incident on a 700 mg/cm^2 secondary ^{9}Be target at 195.7 MeV/u to excite states in ^{34}Cl and ^{31}S after a secondary three proton and a four proton two neutron removal reaction, respectively. Details on the separation and identification of the secondary beam in this experiment can be found in Refs. [6,13]. The time-of-flight through the secondary target was ≈ 23 ps.

5.1. Lineshape of the $1_1^+ \rightarrow 0_{g.s.}^+$ decay in ^{34}Cl

The $1_1^+ \rightarrow 0_{g.s.}^+$ in ^{34}Cl has a known de-excitation energy and halflife of 461 keV and 5.2(3) ps, respectively [12]. However, in the experiment a weak $2_1^+ \rightarrow 1_1^+$ transition was observed with a strength of 12(6)% relative to the $1_1^+ \rightarrow 0_{g.s.}^+$. As the 2_1^+ state has an adopted much longer halflife of 13.7(9) ps [12], the feeding has to be accounted for, resulting in an effective halflife of 6.8(9) ps. The Doppler corrected γ−ray spectra for the Cluster and MINIBALL detectors are shown in Fig. 12. The measured spectrum is compared to simulated spectra assuming halflives of 0, 5, and 20 ps for the excited state. In both cases, experiment and simulation, the same $\langle\beta_{at}\rangle = 0.531$ values and $\langle z_\gamma\rangle = 0$ as target positions were used. The background in the simulations was adopted from the experiment by a linear fit in the region between 400 and 520 keV after subtracting the peak integral. The

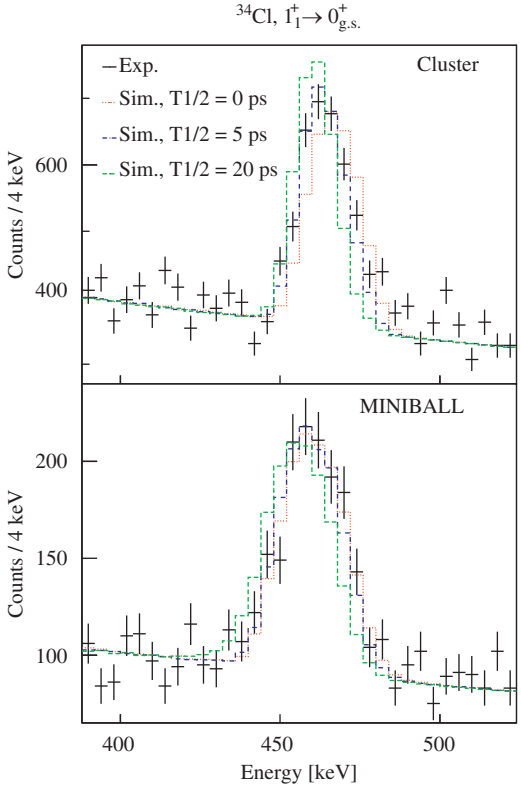

Fig. 12. Doppler corrected Cluster (upper panel) and MINIBALL (lower panel) spectra of the $1_1^+ \rightarrow 0_{g.s.}^+$ in ^{34}Cl. Also shown are the expected line shapes assuming halflives of 0 (red dotted), 5 (blue dashed), and 20 ps (green dash dotted), respectively. (For interpretation of the references to the color in this figure legend, the reader is referred to the web version of this article.)

peak integral of the simulations was normalized separately to the experimentally observed integrals in the Cluster and MINIBALL detectors.

As no attempt was made in the Doppler correction to correct for lifetime effects, the simulated peak energy position clearly shifts as a function of the halflife. A χ^2 test between experiment and simulation was performed. For the simulation the halflife value $T_{1/2}$ of the excited state was varied. Yet always the same $\langle\beta_{at}\rangle$ and $\langle z_\gamma\rangle = 0$ values were used for the Doppler correction. The χ^2 is given by

$$\chi^2 = \sum_{i=1}^{N} \frac{(I^i_{\gamma sim} - I^i_{\gamma exp})^2}{\sigma_i^2} \tag{5}$$

where N is the number of bins, $I^i_{\gamma exp}$ and $I^i_{\gamma sim}$ the number of experimental and simulated counts in the respective bin, and σ_i the statistical error of counts in the respective bin.

The results of the χ^2 test for the observed $1^+_1 \rightarrow 0^+_{g.s.}$ line in ^{34}Cl are shown in Fig. 13. The test was done for 10 energy bins of the Cluster spectrum between 440 and 480 keV and 12 energy bins of the MINIBALL spectrum between 432 and 480 keV. The experimentally observed halflife corresponds to the minimum of the χ^2 distribution. Applying a quadratic fit around the minimum, the error (σ) can be determined from the following equation (see for example Ref. [14], p. 146):

$$\frac{\partial^2\chi^2}{\partial T^2_{1/2}}(T_{1/2} = T^{min}_{1/2}) = \frac{2}{\sigma^2}. \tag{6}$$

Using Eq. (6) results in halflives of 4.0(9) ps and 2.2(20) ps for the Cluster and MINIBALL detectors, respectively, for the $1^+_1 \rightarrow 0^+_{g.s.}$ decay.

Systematic errors may arise mainly from the uncertainty of the position of the detectors relative to the target and the determination of the average β value after the target. As discussed in Sections 4.1 and 4.2, the former affects primarily the MINIBALL array while the latter influences the Cluster detectors. To investigate the systematic errors, two independent sets of simulations were performed. In the first set the target position was shifted by ± 1 mm along the beam axis relative to the γ−ray spectrometers. The resulting simulated χ^2 minimum shifted by ± 0.3 ps for the Cluster detectors and ± 3.6 ps for the MINIBALL detectors, respectively. In the second set of simulations the $\langle\beta_{at}\rangle$ value used for the Doppler correction was shifted by ± 0.001. This resulted in a shift of the χ^2 minimum of -0.7 and $+1.3$ ps for the Cluster detectors, while the shift of the χ^2 minimum for MINIBALL was negligible. The systematic error's asymmetry in the Cluster detector arises from the flat slope of $\langle\beta_{at}\rangle$ towards long halflives, as discussed in Section 2.2, which is also the cause for the asymmetry in the χ^2 distribution.

Thus, for the $1^+_1 \rightarrow 0^+_{g.s.}$ decay in ^{34}Cl values of 4.0 ± 0.9 (stat)$^{+1.3}_{-0.8}$(sys) ps and 2.2 ± 2.0(stat) ± 3.6(sys) ps were found for the Cluster and MINIBALL detectors, respectively, which is lower than the effective halflife that includes feeding contributions. It must be emphasized that the secondary beam energy and target thickness were not designed to measure lifetimes specifically. Furthermore, due to the linear correlation between energy shift and halflife of an excited state, as shown in Fig. 8, the systematic error of the MINIBALL detectors is independent of the halflife, offering an interesting tool to measure halflives ≥ 20 ps. The obtained lifetime results illustrate the additional potential use of the line shape effects at different detection angle. While the Cluster detectors are well suited to draw conclusion on the lifetime and show a distinct χ^2 minimum, the MINIBALL position

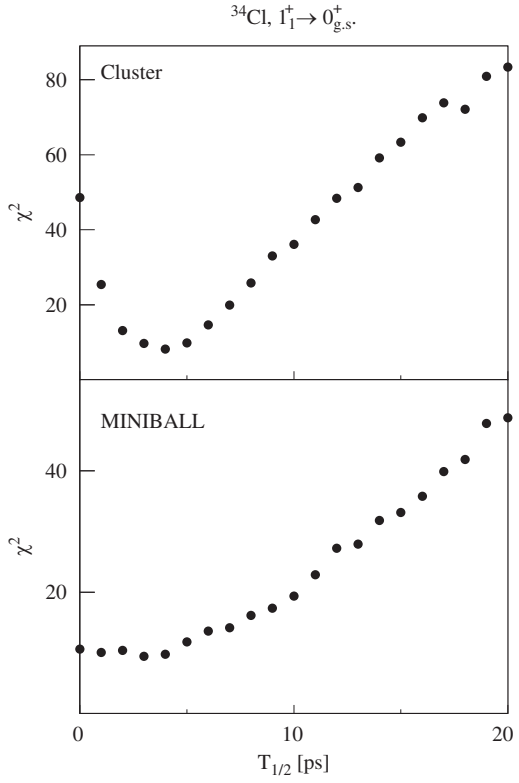

Fig. 13. χ^2 test of the observed $1^+_1 \rightarrow 0^+_{g.s.}$ decay in ^{34}Cl for the Cluster (top panel) and MINIBALL (bottom panel). In the simulations the decay's halflife was varied between 0 and 20 ps in steps of 1 ps.

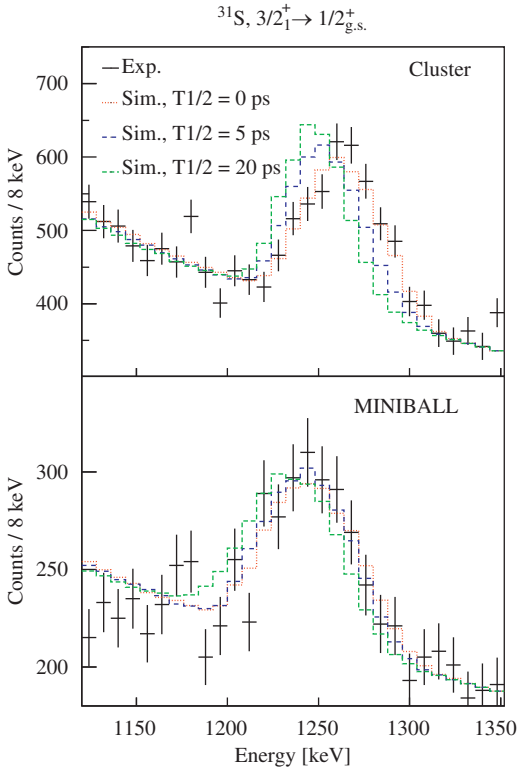

Fig. 14. Doppler corrected Cluster (upper panel) and MINIBALL (lower panel) spectra of the $3/2^+_1 \rightarrow 1/2^+_{g.s.}$ in ^{31}S. Also shown are the expected line shapes assuming halflives of 0 (red dotted), 5 (blue dashed), and 20 ps (green dash dotted), respectively. (For interpretation of the references to the color in this figure legend, the reader is referred to the web version of this article.)

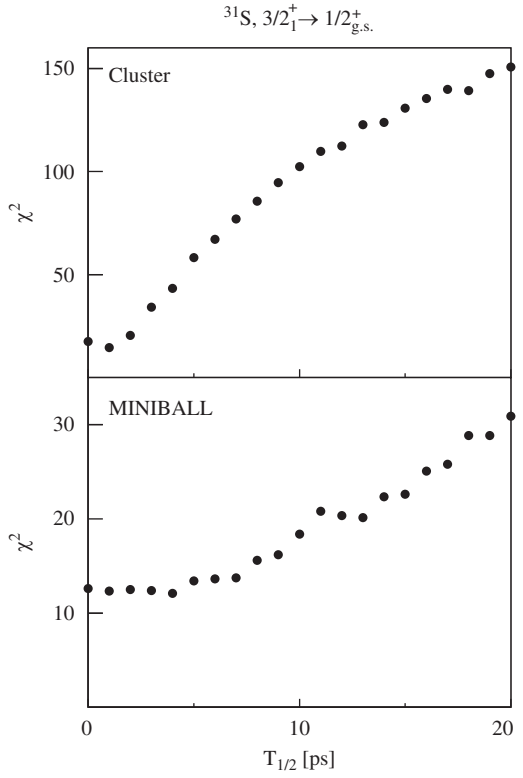

Fig. 15. χ^2 test of the observed $3/2^+_1 \rightarrow 1/2^+_{g.s.}$ decay in ^{31}S for the Cluster (top panel) and MINIBALL (bottom panel). In the simulations the decay's halflife was varied between 0 and 20 ps in steps of 1 ps.

is not sensitive to this quantity as the effective halflife is too short in this case.

5.2. Lineshape of the $3/2^+_1 \rightarrow 1/2^+_{g.s.}$ decay in ^{31}S

As second example the $3/2^+_1 \rightarrow 1/2^+_{g.s.}$ decay in ^{31}S is used to demonstrate the possibility to deduce lifetime information of observed peaks following in-beam γ–ray spectroscopy at relativistic energies. The literature values for energy and halflife are 1249 keV and 500(125) fs, respectively [12]. The Doppler corrected γ–ray spectra are shown in Fig. 14. The same procedure to find the excited state's halflife was repeated. The background was fitted by a linear function in the region in between 1150 and 1350 keV after subtracting the peak integral. The χ^2 test was applied for 13 bins in the region from 1208 to 1312 keV and for 15 bins from 1184 to 1304 keV, for the Cluster and MINIBALL detectors, respectively.

The χ^2 distributions are shown in Fig. 15. Around the χ^2 minimum a quadratic fit was applied, resulting in halflives of $0.8 \pm 0.5(\text{stat})^{+0.9}_{-0.6}(\text{sys})$ ps and $2.2 \pm 3.3(\text{stat}) \pm 3.6(\text{sys})$ ps for the Cluster and MINIBALL detectors, respectively. The systematic errors were deduced in the same way as for the $1^+_1 \rightarrow 0^+_{g.s.}$ decay in ^{34}Cl. Also this example illustrates the potential use of the detected lineshape for lifetime investigations at a much shorter time scale in case the detector positions are well located. Despite the relative error bars the applied method shows that a clear lifetime limit can be stated. A more precise result in analyzing the lineshape of halflives below 1 ps can be obtained in future experiments by employing a target with a higher stopping power per path length, i.e., higher density and atomic number.

6. Conclusions

A precise determination of transition energies in relativistic two-step fragmentation experiments with considerable thick targets needs to consider the lifetime of the γ–decaying state. Uncertainties of the energy measurement are caused by the Doppler correction and its dependence on the change of mean velocity $\langle \beta_\gamma \rangle$ and the decay position $\langle z_\gamma \rangle$ of the emitting excited nucleus. These two observables are typically not accessible in the experiment and cause variation of the energy after Doppler correction and characteristic line shape effects. Here the details of the chosen detector geometry, beam energy, projectile and target nuclei, and target thickness is crucial in order to describe the observed differences to symmetric energy peaks.

In case of a known transition energy of the de-excitation γ–ray the potential use of the described effects is a novel approach for lifetime determination. The explicit and rapid change of lineshape and peak position at different detection angles as a function of lifetime allows fitting of the measured distribution with simulations and applying a χ^2 test. For lifetimes below one ps it is favorable to use high density targets (e.g. Au or Pb) at forward ϑ–angles close to the beam axis. Low density targets as Be or plastic compounds are suitable for lifetimes up to a few tens of ps. Longer lifetimes are best deduced from detectors positioned at $\cos\vartheta_\gamma = \beta_\gamma$ and are nearly independent from the choice of target material. For unknown transition energies a two dimensional χ^2 test is necessary, varying the transition energies and halflives in the simulations.

In the RISING spectrometer the Doppler broadening due to the detectors' opening angles is generally quite large compared to lifetime effects. However, with the advent of the next generation position sensitive γ–ray spectrometers, as AGATA [15] or GRETINA [16], the opening angle will be minimized, thus becoming more sensitive to lineshapes and peak position shifts caused by the lifetimes of excited states in in-beam γ–ray spectroscopy.

Acknowledgments

The authors express their gratitude to the Accelerator Department at GSI for providing the ^{40}Ca beam. One author (P.D.) acknowledges the financial support of the Japan Society for the Promotion of Science. This work was partially supported by the German BMBF under Grant nos. 06BN-109, 06K-167, by the Polish Ministry of Science and Higher Education (Grant nos. N N202 109936 and N N202 309135), and by the Italian Istituto Nazionale di Fisica Nucleare.

References

[1] T. Glasmacher, Ann. Rev. Nucl. Part. Sci. 48 (1998) 1.
[2] F. Azaiez, et al., AIP Conf. Proc. 481 (1998) 243.
[3] H.J. Wollersheim, et al., Nucl. Instr. and Meth. A 537 (2005) 637.
[4] H. Geissel, et al., Nucl. Instr. and Meth. B 70 (1992) 286.
[5] J. Lindhard, A.H. Sørensen, Phys. Rev. A 53 (1996) 2443.
[6] P. Doornenbal, et al., Phys. Lett. B 647 (2007) 237.
[7] J. Eberth, et al., Nucl. Instr. and Meth. A 369 (1996) 135.
[8] J. Eberth, et al., Prog. Part. Nucl. Phys. 46 (2001) 389.
[9] A. Maj, et al., Nucl. Phys. Meth. A 571 (1994) 185.
[10] F. Camera, Ph.D. Thesis, University of Milano, Italy, 1992.
[11] S. Agostinelli, et al., Nucl. Instr. and Meth. A 506 (2003) 250.
[12] ENSDF Database: 〈http://www.nndc.bnl.gov/ensdf〉.
[13] P. Doornenbal, Ph.D. Thesis, University of Cologne, Germany, 2007.
[14] P.R. Bevington, D.K. Robinson, Data Reduction and Error Analysis for the Physical Sciences, second ed., McGraw-Hill, New York, 1992.
[15] J. Simpson, J. Phys. G 31 (2005) S1801.
[16] K. Vetter, et al., Nucl. Phys. Meth. A 452 (2000) 105.